On Retrieval of Inductance and Resistance Dynamics from Experimental Waveforms of a 1 J-class PPT Discharge

IEPC-2024-797

Presented at the 38th International Electric Propulsion Conference, Toulouse, France
June 23-28, 2024

Arsenii Riazantsev*, Maciej Jakubczak†
and Jacek Kurzyna‡
Institute of Plasma Physics and Laser Microfusion, Warsaw, 01-497, Poland

Possibility of recovering resistance and inductance dynamics from the discharge current and voltage waveforms of an electromagnetic Pulsed Plasma Thruster was tested against synthetic and experimental data. Two approaches were used: least squares method with model function represented by Kirchhoff's voltage law of an RLC circuit (or its derivative), formed by the thruster and the plasma discharge, described in terms of capacitors battery voltage (or the discharge current); inverse problem solution of a system of linear equations obtained from finite difference discretization of Kirchhoff's voltage law and its derivative. The least squares method with a model function of linearly changing (with time) resistance and inductance appears to correctly indicate trends of the dynamics of the sought parameters, when applied to synthetic data. Solving the inverse problem appears to be impractical, unless the condition number of the problem is reduced, if possible. Processing of experimental data revealed the presumable existence of current shunting, which complicates the model functions, requiring accurate determination of the shunt current, which is difficult due to uncertain time delay between current and voltage signals. When using least squares method, an alternative approach is possible, which is based on fitting the model function, which does not account for shunting, against the battery's voltage waveform so the found resistance and inductance would correspond to some equivalent circuit of combined plasma and shunt discharge, but not the plasma discharge separately. However, using the latter method against experimental data yields contradicting results.

Nomenclature

κ = condition number
ε = relative error
$\mathbf{A}$ = coefficients matrix of a system of linear equations
$\mathbf{V}$ = covariance matrix
C = capacitance of the battery
I = electric current
I_s = shunt current
L = inductance of the discharge loop
l_1 = linear term of the time-varying inductance
R = resistance of the discharge loop
r_1 = linear term of the time-varying resistance
U = voltage drop of the battery of capacitors

*Research assistant, Department of Plasma Technology, arsenii.riazantsev@ifpilm.pl.
†Research assistant, Department of Plasma Technology, maciej.jakubczak@ifpilm.pl.
‡Research Fellow, Department of Plasma Technology, jacek.kurzyna@ifpilm.pl.

Copyright 2024 by the Electric Rocket Propulsion Society. All rights reserved.

I. Introduction

The idea behind electromagnetic acceleration mechanism of a pulsed plasma thruster (PPT) is analogous to that of a railgun,[1] and relies on the growth of inductance with further advancement of a "projectile" along the acceleration electrodes. The electric configuration of the thruster allows to describe the discharge as a series RLC circuit of variable resistance and inductance, as presented in basic models of PPT such as slug and snowplow.[2,3] Temporal variation of the resistance might be noticeable, taking into account the intricacy of processes in the discharge, however, it is usually ignored in the first approximation. Temporal variation of inductance, in these models, is attributed to position of the plasma current sheet along the acceleration electrodes. However, it can be inferred from numerical simulations that geometric shape of the current sheet itself may affect the inductance, as shown in Figure 1. A situation is conceivable, when the

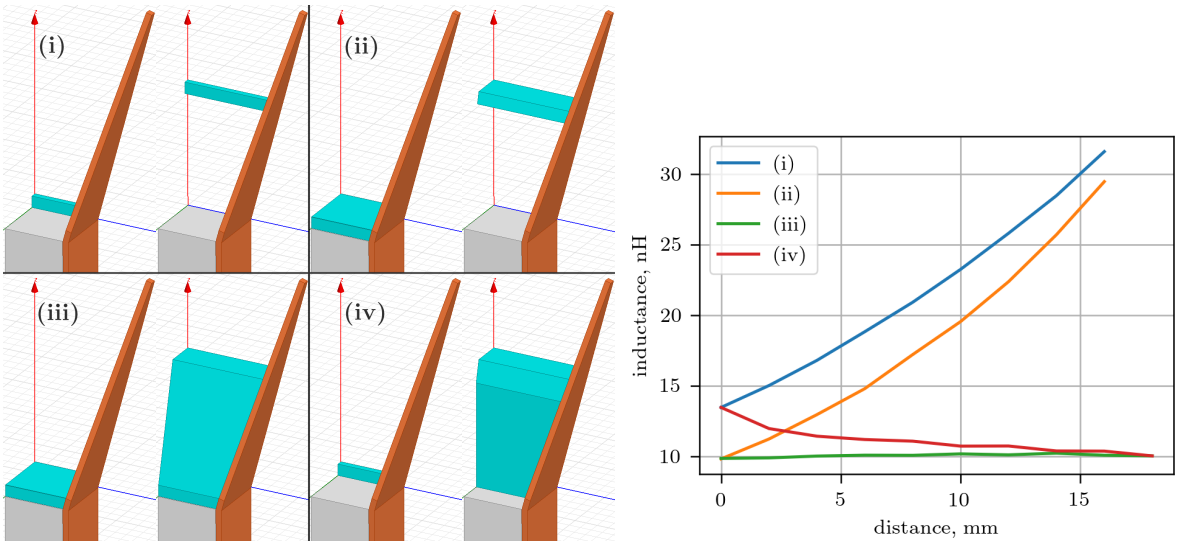

(a) simulated shapes and dynamics of the "plasma" conductor propagation

(b) changes in inductance as "plasma" propagates out of the ablative surface

Figure 1: The results of numerical simulations, aimed to calculate the effect of various shapes (a) of the plasma current sheet (imitated by a copper conductor) on the inductance of the PPT (b). The shape of the conductor and the dynamics of its propagation in each case is as follows: (i) – the cross-section area in the symmetry plane between the electrodes remains the same; (ii) – the length of the cross-section area remains constant but the width decreases together with the electrodes; (iii) – the rear edge of the conductor is always attached to the ablation surface, the front edge moves forward and its width matches the width of electrodes; (iv) – the rear edge of the conductor is always attached to the ablation surface and the conductor expands symmetrically in both directions until the edge of the electrodes.

growth of inductance due to forward advancement of the plasma current sheet is negated by the changes of its structure. In view of this, a question arises concerning possibility to recover the dynamics of resistance and inductance of a PPT discharge from experimental measurements.

Review of previous studies reveals one work[4] in which the resistance was recovered from the discharge current waveform. However, the PPT under investigation was electrothermal, with negligible change of inductance, and resistance was obtained from discharge current values at neighbouring peaks using RLC circuit relations with constant parameters. Number of papers studying electromagnetic PPTs contain comparisons of experimental discharge current/voltage waveforms with some numerical models,[3,5,6] giving consistent results within the assumptions made. At the same time, the fact that PPT modeling can be formally separated into pure electrical (RLC circuit) and pure "mechanical" (plasma acceleration) problems signifies possibility of retrieval experimental dynamics of the parameters of interest without the need for making assumptions about the processes taking place in the plasma discharge.

Experimental data are collected for a 1 J (1 kV) laboratory model of a micro PPT developed at IFPiLM. The laboratory model includes several versions, characterized by different batteries of capacitors of similar total capacitance. An exemplary thruster setup inside a 35 dm^3 vacuum chamber is shown in Figure 2. The

Copyright 2024 by the Electric Rocket Propulsion Society. All rights reserved.

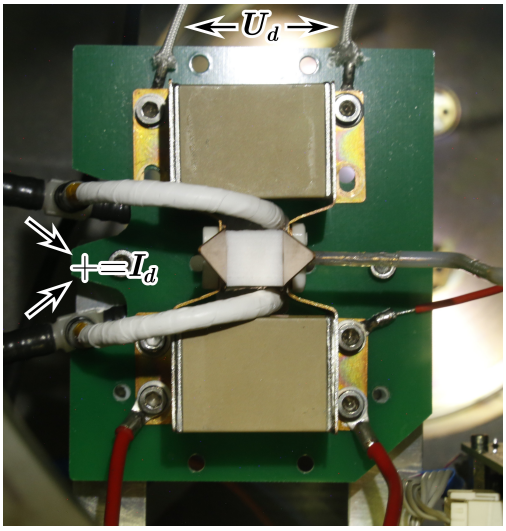

Figure 2: Experimental setup inside the vacuum chamber. The battery consists of 12 Exxelia 180 nF capacitors (C4 dielectric, 2 kV rated voltage). The thruster in the photo is fed with PTFE.

thruster has a copper igniter and tongue-shaped electrodes of length 20 mm and 30° electrode divergence. The interelectrode distance as measured along the ablative surface is 10 mm. It can be fueled either by a solid polytetrafluoroethylene (PTFE) block or liquid perfluoropolyether (PFPE) polymer dispensed in a narrow groove on a surface of a ceramic block. The question of different propellants is out of scope of the paper, hence, later in this paper we consider only PFPE discharges.

The experimental data used in this study were provided with two CWT 60B mini Rogowski transducers applied for discharge current retrieval and high voltage Tektronix THDP0200 differential probe used to measure the potential difference of the capacitors battery. The signals were recorded using 8-bit Tektronix DPO 4104B with 1 GHz bandwidth.

In the present work, we endeavour to extract temporal evolution of the parameters of interest using two approaches: applying least squares method, as described in subsection A; and by discretizing relations of the corresponding RLC circuit and solving the inverse problem, as described in subsection B of the following section. In section III we introduce some technical aspects related to the experiment that prevent the attainment of our objective.

II. Methodology

We start out with Kirchhoff's voltage law for the series RLC circuit of variable resistance and inductance, which reads

$$U - IR - \frac{\mathrm{d}}{\mathrm{d}t}\left(LI\right) = 0. \tag{1}$$

The voltage drop across the capacitors battery U as well as the discharge current I must be known from the experiment. When using the least squares approach the fit can be made against either the voltage or current waveforms, by either writing Equation 1 in terms of U

$$L\frac{\mathrm{d}^2U}{\mathrm{d}t^2} + \left(R + \frac{\mathrm{d}L}{\mathrm{d}t}\right)\frac{\mathrm{d}U}{\mathrm{d}t} + \frac{U}{C} = 0, \tag{2}$$

or by differentiating it with time and writing in terms of I

$$L\frac{\mathrm{d}^2I}{\mathrm{d}t^2} + \left(R + 2\frac{\mathrm{d}L}{\mathrm{d}t}\right)\frac{\mathrm{d}I}{\mathrm{d}t} + \left(\frac{1}{C} + \frac{\mathrm{d}R}{\mathrm{d}t} + \frac{\mathrm{d}^2L}{\mathrm{d}t^2}\right)I = 0. \tag{3}$$

Of course, temporal behavior of resistance and inductance must be assumed. The assumption is not needed when solving the inverse problem, however, both current and voltage waveforms are required in this case.

Copyright 2024 by the Electric Rocket Propulsion Society. All rights reserved.

In order to get the idea about credibility of the approaches, we first test them against synthetically generated waveforms of known (specified by us) temporal behavior of R and L. The waveforms are obtained from numerical integration of one of the above ordinary differential equations (ODEs) as the initial value problem (IVP) using explicit Runge-Kutta method of order 5(4).

A. Least squares fit

In this approach we assume time variation of resistance and inductance to have predominant linear terms: $L(t) = L_0 + l_1 t$ and $R(t) = R_0 + r_1 t$. Equations (2) and (3), in this case, take the form

$$L\frac{\mathrm{d}^2U}{\mathrm{d}t^2} + (R + l_1)\frac{\mathrm{d}U}{\mathrm{d}t} + \frac{U}{C} = 0, \tag{4}$$

and

$$L_0\frac{\mathrm{d}^2I}{\mathrm{d}t^2} + (R + 2l_1)\frac{\mathrm{d}I}{\mathrm{d}t} + \left(C^{-1} + r_1\right) I = 0. \tag{5}$$

The solution is obtained numerically, as a boundary value problem, using SciPy implementation[7] of the fourth order collocation algorithm.[8] By solving the boundary value problem it becomes possible to avoid using data from both current and voltage waveforms, since the initial value problem would require the knowledge about both U and I at the initial time. Finally, the solution of one of the above equations is fit against the experimental current waveform using Trust Region Reflective (TRF) algorithm for bounded problems.[9] The bounds are set so R_0 and L_0 will not become negative or one order larger than the initial guess, while r_1 and l_1 bounds lessen the likelihood of getting negative R and L within the fit interval.

1. *Determination of initial guess*

The initial guess of R_0 and L_0 is obtained using analytical relations for discharge current in RLC circuit of constant parameters. The time interval between the maximum and minimum of the discharge current is the half-period $T/2$, then the resistance and inductance can be found from the relations for decay rate α and angular frequency ω

$$\alpha = \frac{R}{2L} = \frac{2}{T}\ln\left(-\frac{I_{max}}{I_{min}}\right), \tag{6a}$$

$$\omega = \frac{2\pi}{T} = \sqrt{(LC)^{-1} - \alpha^2}. \tag{6b}$$

The initial guess for the linear coefficients r_1 and l_1 is set to zero.

2. *Results*

We start with fitting against synthetic waveforms of linearly changing R and L, the two exemplary results are shown in Figure 3. The fits against both current and voltage waveforms result in negligible maximum residuals $|r|_{max}$. Condition numbers κ are large, in particular, those corresponding to the current waveform exceed those from the voltage waveform by two orders of magnitude. The condition number is calculated from a covariance matrix $\kappa = \|\mathbf{V}^{-1}\|\|\mathbf{V}\|$, obtained from finite difference approximation of Jacobian $\mathbf{V} = s^2\left(\mathbf{J}^T\mathbf{J}\right)$[10,11] of the model function, with s^2 being variance. It is worth to point out that elements of the vector of parameters $[R_0, r_1, L_0, l_1]$ are rescaled to have the same order. When fitting parameters in SI units the condition number drastically increases and the quality of the fit worsens. The uncertainties are estimated from the diagonal terms of the covariance matrix $u_i = \sqrt{V_{i,i}}$. The uncertainties of R_0 and L_0 appear to be smaller than the residual of the fit and the original data. Manually setting the differential step in calculation of the Jacobian matrix seems to have insignificant effect on the covariance matrix.

Fitting the model function of linearly changing resistance and inductance to data with the parameters being changed nonlinearly is done to assess the feasibility of predicting trends of these changes. The test data is synthesised for R and L exponentially increasing/decreasing by half, such that the first derivate tends to zero with time

$$R(t) = R_{t=0}\left(1 \pm \frac{1}{2}\left(1 - e^{-\frac{t}{\tau}}\right)\right), \tag{7a}$$

$$L(t) = L_{t=0}\left(1 \pm \frac{1}{2}\left(1 - e^{-\frac{t}{\tau}}\right)\right). \tag{7b}$$

Copyright 2024 by the Electric Rocket Propulsion Society. All rights reserved.

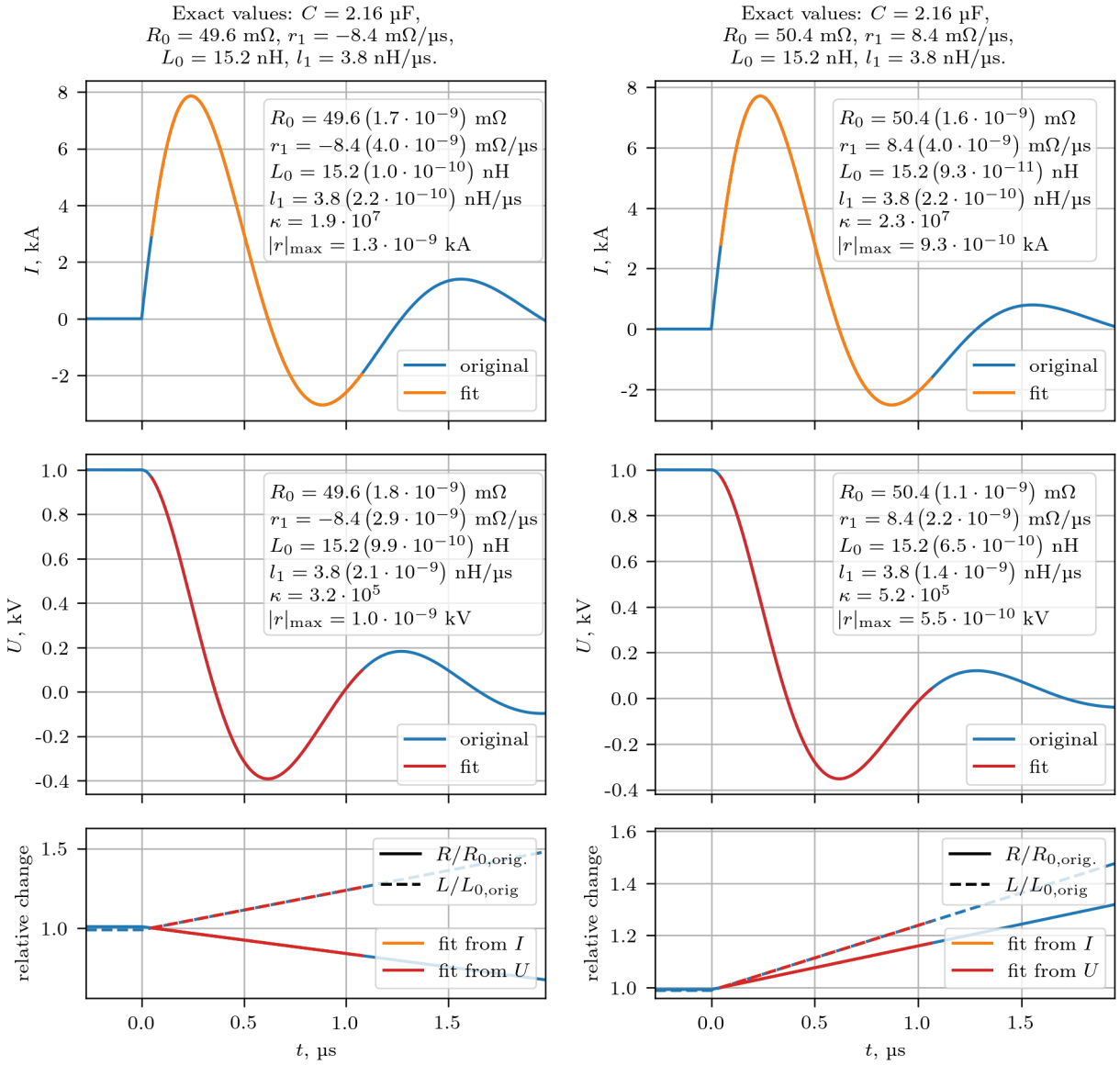

(a) decreasing resistance and increasing inductance

(b) increasing resistance and inductance

Figure 3: Least squares fits of the discharge data of linearly changing resistance and inductance. The obtained parameters are shown in corresponding textboxes. The corresponding uncertainties of the elements of the fit parameters vector $[R_0, r_1, L_0, l_1]$ are enclosed in parentheses.

Copyright 2024 by the Electric Rocket Propulsion Society. All rights reserved.

Time constant in the exponent is chosen to be $\tau = 1.5\pi \left((L_{t=0}C)^{-1} - R_{t=0}(2L_{t=0})^{-1}\right)^{-\frac{1}{2}}$. Figure 4 shows

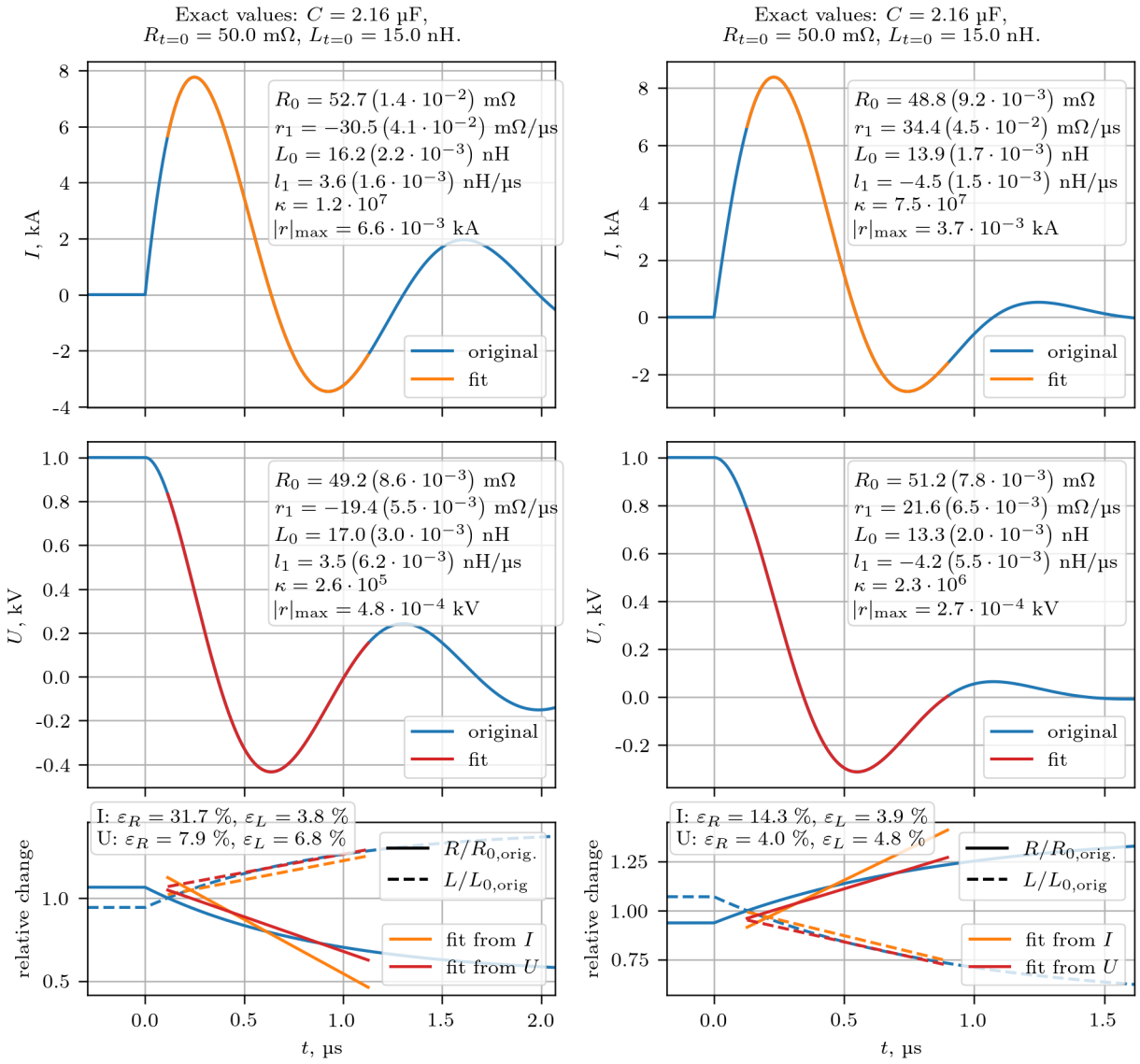

(a) decreasing resistance and increasing inductance

(b) increasing resistance and decreasing inductance

Figure 4: Least squares fits of the discharge data of exponentially changing resistance and inductance. The obtained parameters are shown in corresponding textboxes. The corresponding uncertainties of the elements of the fit parameters vector $[R_0, r_1, L_0, l_1]$ are enclosed in parentheses. The bottommost plot includes relative errors.

that recovered fits correctly represent the trends (growth/decrease) of the original data, but the relative errors are significant. The errors corresponding to resistance seem to be always larger than those corresponding to inductance. A question arises about viability to fit this model function, characterized by linearly changing resistance and inductance, against much smaller neighbouring regions in order to obtain more accurate predictions about the variation of R and L with time. However, reduction of the fit timespans naturally hints at numerical discretization of the ODEs, describing the model, and representing it as a system of linear equations (SLE). The possibility of solving such a SLE is described in the following subsection.

Copyright 2024 by the Electric Rocket Propulsion Society. All rights reserved.

B. Solving inverse problem

1. *System of linear equations*

The central finite difference form of equations 1 and 3 has the form

$$U_n - \left(R_n + \frac{L_{n+1} - L_{n-1}}{2\Delta t}\right) I_n - L_n \frac{I_{n+1} - I_{n-1}}{2\Delta t} = 0, \tag{8a}$$

$$L_n \frac{I_{n+1} - 2I_n + I_{n-1}}{\Delta t^2} + \left(R_n + \frac{L_{n+1} - L_{n-1}}{\Delta t}\right)\left(\frac{I_{n+1} - I_{n-1}}{2\Delta t}\right) + \left(\frac{1}{C} + \frac{R_{n+1} - R_{n-1}}{2\Delta t} + \frac{L_{n+1} - 2L_n + L_{n-1}}{\Delta t^2}\right) I_n = 0. \tag{8b}$$

Rearranging Equation 8 to make ordered pairs of resistance and inductance at subsequent discrete timepoints

$$\overbrace{\frac{I_n}{2\Delta t}}^{a_{i,i-1}} \overbrace{L_{n-1}}^{x_{i-1}} \overbrace{-I_n}^{a_{i,i}} \overbrace{R_n}^{x_i} \overbrace{-\frac{I_{n+1} - I_{n-1}}{2\Delta t}}^{a_{i,i+1}} \overbrace{L_n}^{x_{i+1}} \overbrace{-\frac{I_n}{2\Delta t}}^{a_{i,i+3}} \overbrace{L_{n+1}}^{x_{i+3}} = \overbrace{-U_n}^{b_i}, \tag{9a}$$

$$\overbrace{-\frac{I_n}{2\Delta t}}^{a_{j,j-3}} \overbrace{R_{n-1}}^{x_{j-3}} \overbrace{-\left(\frac{I_{n+1} - 2I_n - I_{n-1}}{2\Delta t^2}\right)}^{a_{j,j-2}} \overbrace{L_{n-1}}^{x_{j-2}} + \overbrace{\left(\frac{I_{n+1} - I_{n-1}}{2\Delta t}\right)}^{a_{j,j-1}} \overbrace{R_n}^{x_{j-1}} + \overbrace{\left(\frac{I_{n+1} - 4I_n + I_{n-1}}{\Delta t^2}\right)}^{a_{j,j}} \overbrace{L_n}^{x_j} + \underbrace{\frac{I_n}{2\Delta t}}_{a_{j,j+1}} \underbrace{R_{n+1}}_{x_{j+1}} + \underbrace{\left(\frac{I_{n+1} + 2I_n - I_{n-1}}{2\Delta t^2}\right)}_{a_{j,j+2}} \underbrace{L_{n+1}}_{x_{j+2}} = \underbrace{-\frac{I_n}{C}}_{b_j}. \tag{9b}$$

One can notice the relation between indices in the above equation $j = i + 1$. It can be inferred from Equation 9 that for N subsequent timepoints (with index n) we obtain a system of $2N$ equations (with index i, coefficients a, and constant terms b), which we rewrite for brevity as

$$f_i = \begin{cases} a_{i,i-1}x_{i-1} + a_{i,i}x_i + a_{i,i+1}x_{i+1} + a_{i,i+3}x_{i+3} = b_i & (i = 2n) \\ a_{i,i-3}x_{i-3} + a_{i,i-2}x_{i-2} + a_{i,i-1}x_{i-1} + a_{i,i}x_i + a_{i,i+1}x_{i+1} + a_{i,i+2}x_{i+2} = b_i & (i = 2n+1) \end{cases}. \tag{10}$$

The system of $2N$ equations has $2N + 4$ unknowns. We can close the system if, for example, the boundary values $R_0 = x_0$, $L_0 = x_1$ and $R_{N+1} = x_{2(N+1)}$, $L_{N+1} = x_{2(N+1)+1}$ are specified. The final system of equations in matrix form becomes

$$\begin{bmatrix} a_{2,2} & a_{2,3} & 0 & a_{2,5} & & & & & \\ a_{3,2} & a_{3,3} & a_{3,4} & a_{3,5} & & & & & \\ & & \ddots & & & & & & \\ & & a_{i,i-1} & a_{i,i} & a_{i,i+1} & 0 & a_{i,i+3} & & \\ & a_{i+1,i-2} & a_{i+1,i-1} & a_{i+1,i} & a_{i+1,i+1} & a_{i+1,i+2} & a_{i+1,i+3} & & \\ & & & & & \ddots & & & \\ & & & & & a_{2N,2N-1} & a_{2N,2N} & a_{2N,2N+1} & \\ & & & & a_{2N+1,2N-2} & a_{2N+1,2N-1} & a_{2N+1,2N} & a_{2N+1,2N+1} & \end{bmatrix} \begin{bmatrix} x_2 \\ x_3 \\ \vdots \\ x_i \\ x_{i+1} \\ \vdots \\ x_{2N} \\ x_{2N+1} \end{bmatrix}$$

$$= \begin{bmatrix} b_2 - a_{2,1}x_1 \\ b_3 - a_{3,0}x_0 - a_{3,1}x_1 \\ \vdots \\ b_i \\ b_{i+1} \\ \vdots \\ b_{2N} - a_{2N,2N+3}x_{2N+3} \\ b_{2N+1} - a_{2N+1,2N+2}x_{2N+2} - a_{2N+1,2N+3}x_{2N+3} \end{bmatrix}, \tag{11}$$

Copyright 2024 by the Electric Rocket Propulsion Society. All rights reserved.

or $\mathbf{Ax} = \mathbf{b}$ for short. The evident drawback of the method is that it requires resistance and inductance at the boundaries to be known. When speaking about experimental data, the parameters can be obtained, for example, at current peaks using least squares method against data of short time span. The question is how the errors in the approximately obtained boundary values might affect the solution? It depends on whether the problem is well or ill-conditioned. One can infer from Equation 11 that condition number of matrix $\mathbf{A}$ cannot be calculated without prior knowledge about current and voltage waveforms, hence, it is individual for every input data.

2. *Results*

The inverse problem is solved for input data from the previous discussions, for both linearly and exponentially changing R and L. The boundary conditions R_0, L_0, R_1, L_1 are taken from exact data. Since matrix $\mathbf{A}$ is sparse and asymmetric, we use direct method based on LU decomposition, implemented within UMFPACK library.[12] The obtained solutions are shown in Figure 5. Recovered temporal evolutions of resistance and

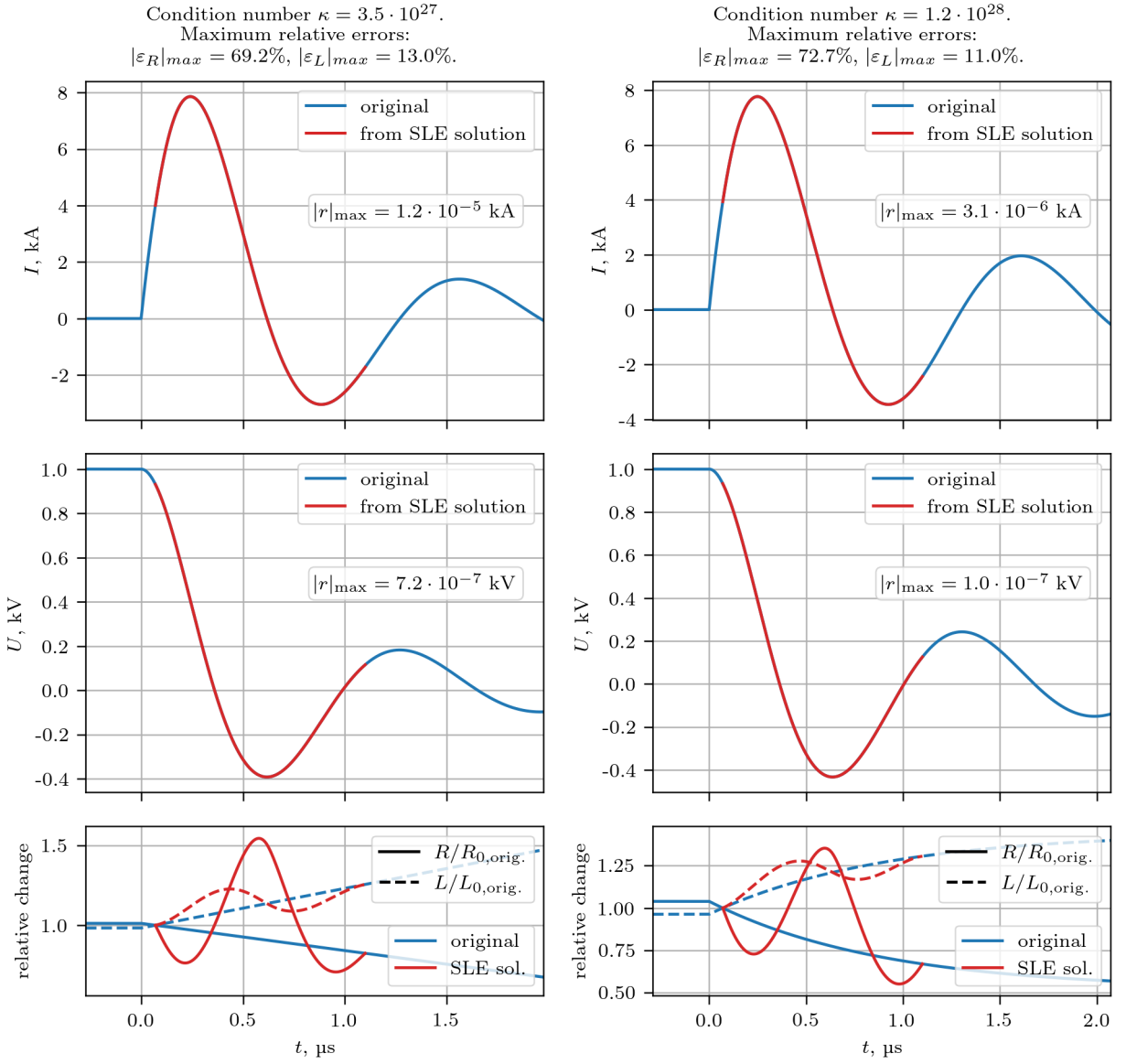

(a) linearly changing R and L

(b) exponentially changing R and L

Figure 5: SLE solutions.

Copyright 2024 by the Electric Rocket Propulsion Society. All rights reserved.

inductance are characterized by noticeable oscillations, nevertheless, the increasing/decreasing trends of the mean values are plain to see. The amplitude of resistance oscillations is around 30% of the initial value. The amplitude of inductance oscillations is at least three times smaller. Numerical integration of Equations 2 and 3, using the retrieved $R(t)$ and $L(t)$ functions approximated for calculations with third order B-splines, gives current and voltage waveforms being very close the original ones with negligible residual. The smallness of the residual between the current and voltage waveforms obtained from the recovered parameters and the original functions hints towards ill-conditionality of the problem. Indeed, as noted in Figure 5 the condition numbers are large. It should be noted that increasing density of discrete data points of the original data (decreasing Δt) has insignificant effect on the recovered resistance and inductance.

III. Fitting PPT discharge waveforms

A. Experiment-related issues

It has been shown that the SLE for solving the inverse problem is highly ill-conditioned, such that the synthetic data solution gives large deviations of the recovered parameters with respect to the original ones. The situation aggravates when solving the inverse problem for experimental data due to inaccuracies in measurements, not least of which is the delay between the current and voltage waveforms. In an attempt to identify this delay, by integrating the current signal with time and correlating the integral with the voltage waveform, we come upon inconsistency between both signals, as shown in Figure 6 where the amplitudes of the first minimum do not match even when the nominal capacitance is corrected by a factor, lying within the manufacturers tolerance (180±10% nF, Exxelia C487 capacitors, 2kV rated voltage), to force the integral's potential drop to agree with the voltage probe measurement. There are two possible explanations

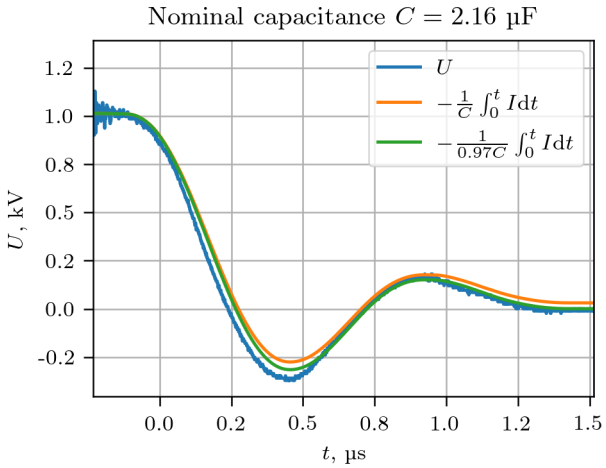

Figure 6: Comparison of the capacitors voltage and the integrated discharge current. The green line shows the result when the capacitance is being scaled such that the integrated voltage drop agrees with the voltage probe measurement, but due to possible current shunting this might not be the case.

of this inconsistency. The first is the distortion of measured signals due to frequency response or slew rate limitations of the probes. The second is the current shunting which might appear when a part of the discharge current is not being captured by Rogowski transducers, for example, a charge flowing on the surface of the capacitors (see Figure 2). As mentioned in section I, the current is measured using two CWT 60B mini Rogowski transducers and voltage is measured using Tektronix THDP0200 differential probe. Compared to approximately 1 MHz frequency of the discharge oscillations, the transducers of 16 MHz bandwidth and the probe of 200 MHz bandwidth have negligibly small losses of sensitivity. The slew rate of the current transducers is 40 kA/µs, whereas the maximum $\mathrm{d}I/\mathrm{d}t$ is calculated to be 20 kA/µs. The slew rate of the voltage probe is 650 kV/µs, whereas maximum $\mathrm{d}U/\mathrm{d}t$ from Figure 6 is two orders smaller (around 4 kV/µs).

As the operational limits of the measuring instruments are not exceeded, the assumption about the existence of the shunting current remains open for acceptance. The electric circuit with current shunting can be described as in Figure 7 and the Kirchhoff circuit laws give three equations: one for current at the nodes

Copyright 2024 by the Electric Rocket Propulsion Society. All rights reserved.

and two for the voltage drops along the loops. The differential equations describing the capacitors voltage

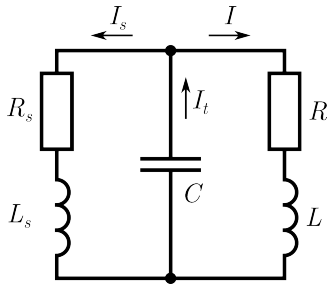

Figure 7: Schematic diagram of RLC circuit with shunting.

U and the plasma discharge current I become inhomogeneous

$$L\frac{\mathrm{d}^2U}{\mathrm{d}t^2} + \left(R + \frac{\mathrm{d}L}{\mathrm{d}t}\right)\frac{\mathrm{d}U}{\mathrm{d}t} + \frac{U}{C} = -\frac{1}{C}\left[L\frac{\mathrm{d}I_s}{\mathrm{d}t} + \left(R + \frac{\mathrm{d}L}{\mathrm{d}t}I_s\right)\right], \tag{12a}$$

$$L\frac{\mathrm{d}^2I}{\mathrm{d}t^2} + \left(R + 2\frac{\mathrm{d}L}{\mathrm{d}t}\right)\frac{\mathrm{d}I}{\mathrm{d}t} + \left(\frac{1}{C} + \frac{\mathrm{d}R}{\mathrm{d}t} + \frac{\mathrm{d}^2L}{\mathrm{d}t^2}\right)I = -\frac{I_s}{C}. \tag{12b}$$

The inhomogeneous term in Equation 12a contains the shunt current I_s and its first derivative, let alone the sought parameters R and L. Even if it were possible to recover I_s from the current and voltage waveforms it would be the most convenient to fit Equation 12b, as it does not include derivative of the shunt current, therefore, introduces less noise. Determination of I_s can be avoided by considering an equivalent one-loop RLC circuit, such that ODE describing the system is analogous to Equation 1 but the current flowing through the loop is $I_t = I + I_s = -C\frac{\mathrm{d}}{\mathrm{d}t}U$ and the variable coefficients of the equation are R_{eq} and L_{eq}.

The presence of current shunting additionally complicates the task of finding R and L dynamics. Solution of inverse problem is affected to a greater extent, as it is more susceptible to inaccuracies. One could think of modification of Equation 8 by representing discharge current in terms of U to build a SLE for the one-loop equivalent circuit and solving the SLE for R_{eq} and L_{eq}. This approach would introduce third-order derivative of the capacitors voltage, but will not increase the number of variables required to close the system as U is known and is used to build the coefficients matrix $\mathbf{A}$ and the "constant" terms vector $\mathbf{b}$. However, the approach would increase the numerical differentiation error. Under the circumstances, the least squares method remains to be more reasonable option.

B. Least squares fit of experimental data

The technical difficulties in finding the shunt current make fitting against the capacitors voltage waveform using least squares method to be the only viable approach, which, at least, might show the trends in the dynamics of the equivalent circuit parameters. Two exemplary results are shown in Figure 8. Both fits are made for the same original data but for different timespans. The fits are made against raw voltage waveform, however, since the model function is represented by a boundary value problem, the boundary values U_0 and U_1 are taken from filtered signal. Given the same initial data, except for the timespan under fit, the resultant resistance and inductance trends in these two examples are opposite. It is hard to say about the resistance, but the decrease of inductance in Figure 8b contradicts with the plasma acceleration principle of an electromagnetic PPT. Mass spectrometry analysis[13,14] as well as fast photography of the exhaust plume[15] confirm the exhaust particles to be accelerated above thermal speeds. The fit in Figure 8b gives increasing inductance, but the condition number is almost five orders higher than that from the fit in Figure 8a. The maximum residuals in both cases are comparable. It is worth to point out that fitting different timespans of the synthetic data with nonlinearly changing R and L (exponentially, in that case) always detects the trends of these changes correctly. Moreover, the relative error of the obtained inductance is usually small compared to the relative error of the resistance. Another difference between the experimental and synthetic data is that the capacitance of the battery is not known precisely and, as was mentioned previously, may vary by 10%. However, variations of the capacitance by 10% affect the determined initial guess but the relative changes of the recovered parameters remain the same.

Copyright 2024 by the Electric Rocket Propulsion Society. All rights reserved.

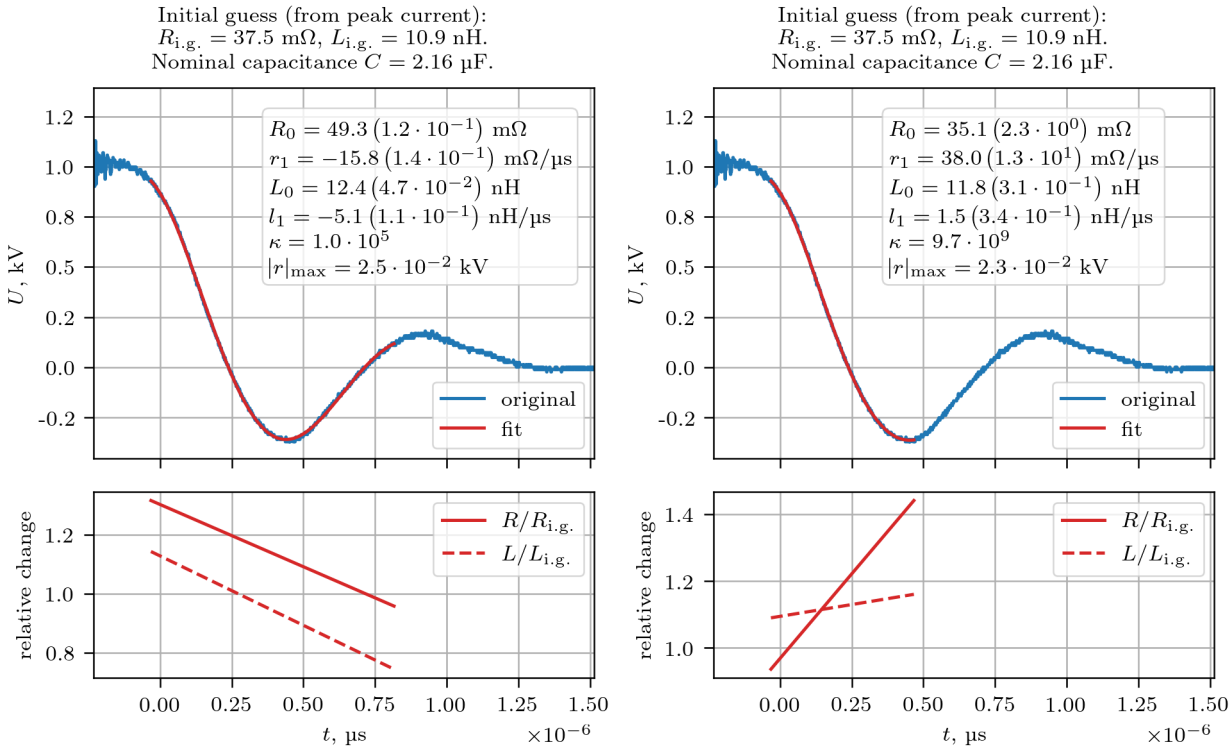

(a) longer timespan but smaller condition number

(b) shorter timespan but larger condition number

Figure 8: Least squares fits of the experimental voltage waveform of linearly increasing resistance and inductance. The obtained parameters are shown in corresponding textboxes. The corresponding uncertainties of the elements of the fit parameters vector $[R_0, r_1, L_0, l_1]$ are enclosed in parentheses.

IV. Conclusions

Among the two presented methods of retrieval of resistance and inductance dynamics, the least squares fit appears to be more insightful, when testing against synthetically generated data. The inverse problem solution, that was initially considered to be highly promising, appears to provide uncertain data as can be inferred when applying to test data and from the extremely large condition number. Under the circumstances, application of the method on the experimental data seems impractical, unless the SLE can be restated to reduce the condition number of the matrix of coefficients $\mathbf{A}$ (maybe by formulating the problem in dimensionless form, as it significantly improves condition number and quality of the least squares method results). Fitting of experimental data using least squares method against the voltage waveform and for the equivalent circuit (ignoring the inhomogeneity of the problem, due the presence of current shunting) gives contradictory results. This behavior is not observed when applied to synthetic data. It remains an open question, whether accurate identification of the shunt current and fitting against the current waveform with the model function based on inhomogeneous ODE (Equation 12b) would provide the results that do not contradict with the mechanism of electromagnetic plasma acceleration and with the fits made for different timespans.

Acknowledgments

The study was carried out within "Pulsed plasma thruster for nano and micro satellites" project, funded by the National Centre for Research and Development (Grant Agreement No. POIR.01.01.01-00-0857/19). The authors would to thank the industrial partner Liftero sp. z o.o. (formerly Progresja Space sp. z o.o.; especially Przemysław Drożdż, Marcin Chuchla, and Grzegorz Bywalec) for their contribution in designing and manufacturing of the thruster components. The authors also would like to acknowledge Semicon sp. z

Copyright 2024 by the Electric Rocket Propulsion Society. All rights reserved.

o.o. (in particular Piotr Ciszewski and Grzegorz Pasek) for their help with reflow soldering of the capacitors batteries.

References

[1]McDonald, K., "Capacitor-Driven Railgun: Magnetic Fields Doing Work," 2017.

[2]Wagner, H. and Auweter-Kurtz, M., "Slug Model and Snowplow Model for Pulsed Plasma Thruster Description," *40th AIAA/ASME/SAE/ASEE Joint Propulsion Conference and Exhibit*, American Institute of Aeronautics and Astronautics, June 2004.

[3]Mikellides, P. G., Henrikson, E. M., and Rajagopalan, S. S., "Theoretical Formulation for the Performance of Rectangular, Breech-Fed Pulsed Plasma Thrusters," *Journal of Propulsion and Power*, Vol. 35, No. 4, 2019, pp. 811–818.

[4]Wang, Y., Ding, W., Cheng, L., Yan, J., Li, Z., Wang, J., and Wang, Y., "An Investigation of Discharge Characteristics of an Electrothermal Pulsed Plasma Thruster," *IEEE Transactions on Plasma Science*, Vol. 45, No. 10, 2017, pp. 2715–2724.

[5]Shaw, P. and Lappas, V., "Modeling of a Pulsed Plasma Thruster; Simple Design, Complex Matter," 2010.

[6]Ou, Y., Wu, J., Zhang, Y., Li, J., and Tan, S., "Theoretical Modeling and Parameter Analysis of Micro-Pulsed Plasma Thruster," *Energies*, Vol. 11, No. 5, May 2018, pp. 1146.

[7]Virtanen, P., Gommers, R., Oliphant, T. E., Haberland, M., Reddy, T., Cournapeau, D., Burovski, E., Peterson, P., Weckesser, W., Bright, J., van der Walt, S. J., Brett, M., Wilson, J., Millman, K. J., Mayorov, N., Nelson, A. R. J., Jones, E., Kern, R., Larson, E., Carey, C. J., Polat, İ., Feng, Y., Moore, E. W., VanderPlas, J., Laxalde, D., Perktold, J., Cimrman, R., Henriksen, I., Quintero, E. A., Harris, C. R., Archibald, A. M., Ribeiro, A. H., Pedregosa, F., van Mulbregt, P., and SciPy 1.0 Contributors, "SciPy 1.0: Fundamental Algorithms for Scientific Computing in Python," *Nature Methods*, Vol. 17, 2020, pp. 261–272.

[8]Kierzenka, J. and Shampine, L. F., "A BVP solver based on residual control and the Maltab PSE," *ACM Trans. Math. Softw.*, Vol. 27, No. 3, sep 2001, pp. 299–316.

[9]Branch, M. A., Coleman, T. F., and Li, Y., "A Subspace, Interior, and Conjugate Gradient Method for Large-Scale Bound-Constrained Minimization Problems," *SIAM Journal on Scientific Computing*, Vol. 21, No. 1, 1999, pp. 1–23.

[10]Vugrin, K. W., Swiler, L. P., Roberts, R. M., Stucky-Mack, N. J., and Sullivan, S. P., "Confidence region estimation techniques for nonlinear regression in groundwater flow: Three case studies," *Water Resources Research*, Vol. 43, No. 3, 2007.

[11]Aster, R. C., Borchers, B., and Thurber, C. H., *Parameter Estimation and Inverse Problems*, Elsevier, Oct. 2018.

[12]Davis, T. A., "Algorithm 832: UMFPACK V4.3—an unsymmetric-pattern multifrontal method," *ACM Trans. Math. Softw.*, Vol. 30, No. 2, jun 2004, pp. 196–199.

[13]Jakubczak, M., Jardin, A., and Kurzyna, J., "Plasma plume composition of a pulsed plasma thruster fed with perfluoropolyether," IEPC-2024-336, 06 2024.

[14]Jakubczak, M., Jardin, A., and Kurzyna, J., "Analysis of composition and dynamics of the plasma plume emitted by a 1 J pulsed plasma thruster fed with polytetrafluoroethylene and determination of thruster efficiency components," *Physics of Plasmas*, Vol. 31, No. 5, 05 2024, pp. 053501.

[15]Riazantsev, A., Jakubczak, M., Cichorek, O., and Kurzyna, J., "Side and Front Imaging of Plasma Discharge Evolution in an Ablative Pulsed Plasma Thruster Operated with Solid and Liquid Propellants," (To be published).

Copyright 2024 by the Electric Rocket Propulsion Society. All rights reserved.